

Fabry-Pérot Interferometry at the $\nu = 2/5$ Fractional Quantum Hall State

J. Nakamura,^{1,2} S. Liang,^{1,2} G. C. Gardner,^{2,3} and M. J. Manfra^{1,2,3,4,5,*}


¹*Department of Physics and Astronomy, Purdue University, West Lafayette, Indiana 47907, USA*

²*Birck Nanotechnology Center, Purdue University, West Lafayette, Indiana 47907, USA*

³*Microsoft Quantum Lab West Lafayette, West Lafayette, Indiana 47907, USA*

⁴*Elmore Family School of Electrical and Computer Engineering, Purdue University, West Lafayette, Indiana 47907, USA*

⁵*School of Materials Engineering, Purdue University, West Lafayette, Indiana 47907, USA*

 (Received 18 April 2023; revised 1 August 2023; accepted 22 August 2023; published 23 October 2023)

Electronic Fabry-Pérot interferometry is a powerful method to probe quasiparticle charge and anyonic braiding statistics in the fractional quantum Hall regime. We extend this technique to the hierarchy $\nu = 2/5$ fractional quantum Hall state, possessing two edge modes that in our device can be interfered independently. The outer edge mode exhibits interference similar to the behavior observed at the $\nu = 1/3$ state, indicating that the outer edge mode at $\nu = 2/5$ has properties similar to the single mode at $\nu = 1/3$. The inner mode shows an oscillation pattern with a series of discrete phase jumps indicative of distinct anyonic braiding statistics. After taking into account the impact of bulk-edge coupling, we extract an interfering quasiparticle charge $e^* = 0.17 \pm 0.02$ and anyonic braiding phase $\theta_a = (-0.43 \pm 0.05) \times 2\pi$, which serve as experimental verification of the theoretically predicted values of $e^* = \frac{1}{5}$ and $\theta_a = -(4\pi/5)$.

DOI: [10.1103/PhysRevX.13.041012](https://doi.org/10.1103/PhysRevX.13.041012)

Subject Areas: Condensed Matter Physics,
Quantum Physics,
Strongly Correlated Materials

I. INTRODUCTION

The fractional quantum Hall effect [1] is the archetype of a strongly interacting topological phase of matter hosting anyonic excitations. Quantum Hall states at fractional filling factors of the form $\nu = (1/2p + 1)$ are described by the Laughlin wave function [2]. Higher-order fractional states $\nu = (n/2pn + 1)$ (n, p integers) may be understood in terms of the hierarchical construction [3,4] or the composite fermion model [5–7]. The elementary excitations of fractional quantum Hall states are quasiparticles carrying a fraction of an electron's charge [2] and obeying anyonic braiding statistics [4,8–11]. At the $\nu = 1/3$ Laughlin state, fractional charge has been observed through resonant tunneling [12,13], shot noise [14,15], scanning single electron transistor techniques [16], and interference [17], while evidence for anyonic statistics has been observed with Fabry-Pérot interferometry [18,19], in quasiparticle collision experiments [20–22], and recently in Mach-Zehnder interferometers [23].

It is natural to attempt to extend experimental probes of exotic statistics to the hierarchy state $\nu = 2/5$, one of the principal daughter states of $\nu = 1/3$. In the collider geometry, recent shot-noise cross-correlation experiments have reported novel behavior at $\nu = 2/5$ [21,22], providing evidence for sensitivity to statistical properties of $e/5$ quasiparticles, where e is the charge of an electron. Two-particle time-domain shot-noise experiments indicate that quantum coherence can be maintained for $e/5$ anyons at $\nu = 2/5$ [24]. Theoretically, Mach-Zehnder interferometry provides a method to probe the statistics of edge quasiparticles via interference visibility [25–27] and may also be sensitive to non-Abelian statistics [28]. Electronic Fabry-Pérot interferometry is a powerful probe of quasiparticle charge and statistics and has been studied in numerous theoretical [27,29–40] and experimental works [41–51], with recent experiments extending the measurement technique to the quantum Hall effect in graphene [52–54].

Here we describe the operation of a Fabry-Pérot interferometer and quantitative analysis of braiding statistics at $\nu = 2/5$. There are challenges to extending interferometry to more fragile, higher-order states. The energy gap at $\nu = 2/5$ is significantly smaller than at $\nu = 1/3$, making it important to use a high-quality heterostructure with reasonably high electron density so that an incompressible state can be achieved both in the bulk 2DEG and in a confined device. Also, $\nu = 2/5$ is expected to have two

*mmanfra@purdue.edu

Published by the American Physical Society under the terms of the [Creative Commons Attribution 4.0 International license](https://creativecommons.org/licenses/by/4.0/). Further distribution of this work must maintain attribution to the author(s) and the published article's title, journal citation, and DOI.

distinct charged edge modes, making it important to independently interfere both the inner and outer modes. At $\nu = 2/5$, the bulk quasiparticles and the tunneling charge on the inner edge mode are expected to carry fractional charge $e/5$ [6,7,55,56]. The expected value of the anyonic phase for braiding one $e/5$ quasiparticle around another (or exchanging positions twice) is $\theta_a = -2\pi \times (2p/2pn + 1)$, yielding $\theta_a = -2\pi \times \frac{2}{5}$ [4,55,57,58]. Our measurements and analysis demonstrate that Fabry-Pérot interferometry may be used to quantitatively determine fractional charge and anyonic braiding statistics in complex multi-edge-mode fractional quantum Hall states and hold promise for study of putative non-Abelian states as well.

A quantum Hall Fabry-Pérot interferometer uses two quantum point contacts (QPCs) to partially reflect incident edge states which propagate around the gate-defined edge of the 2DEG. Interference occurs between coherent waves backscattered at each of the QPCs. In the limit of weak backscattering, the quantum Hall interferometer generates a phase difference given by Eq. (1) [31,55]:

$$\frac{\theta}{2\pi} = e^* \frac{AB}{\Phi_0} + N_{\text{QP}} \frac{\theta_a}{2\pi}. \quad (1)$$

Note that this interference phase is for counterclockwise propagation of a quasiparticle around the loop with magnetic field in the $-\hat{z}$ direction. Equation (1) includes the Aharonov-Bohm (AB) phase and the anyonic phase contribution θ_a , with N_{QP} the number of quasiparticles localized inside the interferometer. e^* is the dimensionless ratio of the quasiparticle charge to the bare electron charge, B is the magnetic field, and A is the area of the interference path around which the edge states circulate; this area is defined by the QPC gates and side gates. $\Phi_0 \equiv (h/e)$ is the magnetic flux quantum. A list of symbols is given in Table 1 in the Supplemental Material [59]. For $\nu = 1/3$, theory predicts $e^* = \frac{1}{3}$ and $\theta_a = (2\pi/3)$, while for $\nu = 2/5$, $e^* = \frac{1}{5}$ and $\theta_a = (-4\pi/5)$ [4,11,35,55,58,60,61]. Note that the charge $e/5$ at $\nu = 2/5$ is associated with localized quasiparticles in the bulk and the tunneling charge on the inner edge mode. The outer edge belonging to the lowest composite fermion Lambda level [5,7] is expected to support charge $e/3$ quasiparticles, as at $\nu = 1/3$. This has been confirmed in shot-noise experiments [56].

If the chemical potential is in an energy gap so that the bulk is incompressible and the quasiparticle number is fixed as B and side gate voltage V_{SG} are varied, then the conductance G will oscillate with a flux period of Φ_0/e^* . At fixed filling factor, increasing magnetic field increases the number of electrons in the quantum Hall condensate, equal to $\nu AB/\Phi_0$. At specific values of B and V_{SG} , local variations in the disorder potential landscape may favor the addition of a holelike quasiparticle (or the removal of an electronlike quasiparticle) inside the bulk rather than the continuous addition of charge that keeps the filling factor

fixed, leading to a discrete change in phase by $-\theta_a$. Note that $\nu = 2/5$ has smaller quasiparticle charge compared to $\nu = 1/3$, making the Aharonov-Bohm phase evolve more gradually with changes in magnetic field, and a larger magnitude of θ_a ; these two factors will make the discrete jumps in phase when the quasiparticle number changes a more dramatic effect than at $\nu = 1/3$, since the anyonic phase contribution is much larger relative to the slowly varying Aharonov-Bohm component.

Equation (1) neglects the effects of bulk-edge coupling, which can cause the area of the interference path to change when charge in the bulk changes (either in the condensate or in the form of localized quasiparticles). In the presence of finite bulk-edge coupling, the interference phase will be modified [36,38,55]:

$$\frac{\theta}{2\pi} = e^* \frac{\bar{A}B}{\Phi_0} - \kappa \frac{e^*}{\Delta\nu} \left(e^* N_{\text{QP}} + \nu_{\text{in}} \frac{\bar{A}B}{\Phi_0} - \bar{q}_b \right) + N_{\text{QP}} \frac{\theta_a}{2\pi}. \quad (2)$$

In Eq. (2), \bar{A} is the ideal area of the interference path (not including variations δA due to the bulk-edge coupling), $\Delta\nu$ is the difference between the filling factor corresponding to the interfering edge state and the filling factor of the next-outer fully transmitted edge state, ν_{in} is the filling factor corresponding to the interfering edge state, and \bar{q}_b is the charge of ionized impurities and induced charge on the metallic gate resulting from the applied gate voltages. $\kappa \equiv -(\delta q_i / \delta q_b)$ is the effective bulk-edge coupling parameter which describes how much the charge on the interfering edge mode (q_i) changes (and thus area changes) in response to a change in bulk charge [the total excess bulk charge is the term in parentheses in Eq. (2), $\delta q_b \equiv e^* N_{\text{QP}} + \nu_{\text{in}} (\bar{A}B/\Phi_0) - \bar{q}_b$]. Note that q_b and q_i are measured in units of the bare electron charge e .

II. MEASUREMENTS AT $\nu = 1$

The primary device studied in this work, labeled device A, consists of two QPCs which partially reflect edge modes, and a pair of side gates to define an interference path. An SEM image of an identical device is shown in Fig. 1(a). This device has lithographic dimensions $1 \times 1 \mu\text{m}^2$, and is fabricated on a GaAs/AlGaAs heterostructure utilizing the screening well design similar to our previous experiments [17]; this heterostructure reduces bulk-edge coupling, making it possible to observe the anyonic phase when the localized quasiparticle number changes [18]. The degree of residual bulk-edge coupling is controlled through heterostructure and device design [19]. The heterostructure and device are detailed in Supplemental Material Fig. 1 and Sec. I [59] (simulations are done with the NEXTNANO software package [62]). The electron density is $n \approx 1.05 \times 10^{11} \text{ cm}^{-2}$ and mobility $\mu \approx 9 \times 10^6 \text{ cm}^2/\text{V} \cdot \text{s}$. Note that this density is

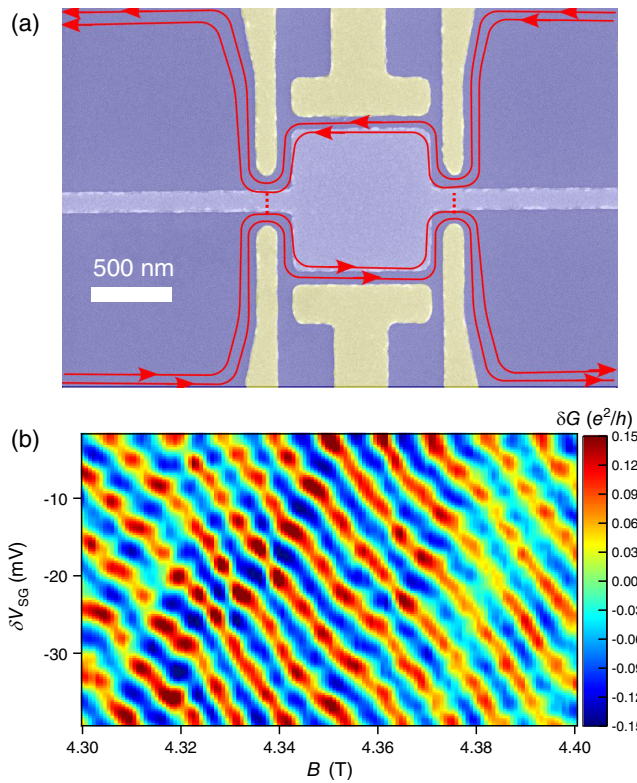


FIG. 1. (a) False-color SEM image of an interferometer with the same dimensions as the device used in our experiment. Red lines indicate propagating edge states. The illustrated configuration corresponds to the case of $\nu = 2/5$, where there are two edge states. (b) Conductance oscillations at $\nu = 1$ versus magnetic field and side gate voltage V_{SG} . The negatively sloped lines of constant phase indicate Aharonov-Bohm regime behavior, while weak modulations suggest small but finite bulk-edge coupling.

higher than in previous devices used to probe braiding at $\nu = 1/3$ [18,19]; higher density enables a more robust $\nu = 2/5$ state. Conductance measurements are made using standard lock-in amplifier techniques with a typical excitation voltage of $10 \mu\text{V}$ and frequency of 13 Hz , and are performed in a dilution refrigerator at a temperature of $T = 10 \text{ mK}$ except where otherwise noted.

Figure 1(b) shows conductance variation δG (with a smooth background subtracted) versus magnetic field B and side-gate-voltage variation δV_{SG} at the integer quantum Hall state $\nu = 1$. Note that ΔV_{SG} is relative to -1.8 V in all measurements, and the side-gate-voltage excursions around this value are small so that the area changes by only a few percent. Since at $\nu = 1$ the dominant tunneling charge is the electron, the interference phase will be determined by the AB phase in Eq. (1), and the oscillation period will be Φ_0 , making it possible to extract the effective area of the interferometer and the lever arm $\partial \bar{A} / \partial V_{SG}$ relating a change in gate voltage to change in area (see Supplemental Material Sec. II and Fig. 2 [59]). Negatively sloped lines

of constant phase are a signature of Aharonov-Bohm interference [36,44,55], while weak modulations in the pattern suggest small but finite bulk-edge coupling. The magnetic field period $\Delta B = 11 \text{ mT}$ gives the effective area $A = (\Phi_0 / \Delta B) \approx 0.38 \mu\text{m}^2$. This indicates an approximate depletion length of 200 nm around the gates, consistent with previous measurements and simulations of similar devices [17–19]. The gate-voltage oscillation period is $\Delta V_{SG} = 8.5 \text{ mV}$ yielding $(\partial \bar{A} / \partial V_{SG}) = (\Phi_0 / B \Delta V_{SG}) = 0.11 \mu\text{m}^2 \text{ V}^{-1}$.

III. MEASUREMENTS AT $\nu = 2/5$

In Fig. 2(a), we show measurements of the bulk Hall resistance R_{xy} (black) at high magnetic field in the fractional quantum Hall regime, measured in a region of 2DEG away from the interferometer. Prominent resistance plateaus occur at $\nu = 1/3$ and $\nu = 2/5$. Measurement of the diagonal resistance across the device R_D is displayed in red, with a small negative voltage of -0.3 V on the QPCs and side gates in order to deplete the electrons under the gates but not induce significant backscattering in the QPCs. Given any backscattering in the device, R_D will generally be higher than R_{xy} , but note there is a wide range of magnetic field at $\nu = 1/3$ where $R_D \approx 3(h/e^2)$ while the R_{xy} remains quantized, indicating nearly full transmission of the edge state through the device. At $\nu = 2/5$, there is a range of magnetic field approximately 200 mT wide where $R_D \approx 2.5(h/e^2)$, indicating that both edge modes are nearly fully transmitted through the device with minimal conduction through the bulk.

In Fig. 2(b), we show conductance versus QPC gate voltage for the two QPCs individually at $\nu = 2/5$. There is a wide primary plateau with $G \approx 0.4e^2/h$ where both edge modes are nearly fully transmitted through the device. As V_{QPC} is made more negative, conductance decreases and then reaches a second, intermediate plateau at $G \approx \frac{1}{3}(e^2/h)$, indicating that the inner edge state is fully reflected while the outer one (which carries conductance $\frac{1}{3}(e^2/h)$) is fully transmitted. Beyond this second plateau, the outer edge state starts to be reflected, and conductance drops until reaching zero. Tuning the QPCs to values between the first and second plateaus corresponds to partial reflection of the inner mode, while tuning conductance between the second plateau and zero conductance corresponds to partially reflecting the outer edge mode while the inner one is fully reflected; thus, it is possible to set V_{QPC} on both QPCs to select which edge mode is interfered. This *in situ* tuning of individual edge mode transmission is critical to our experiment. Approximate gate operating points for interference of the inner mode and outer mode are indicated with arrows in the figure (these points are not exact since there is a small amount of cross-coupling between the gates).

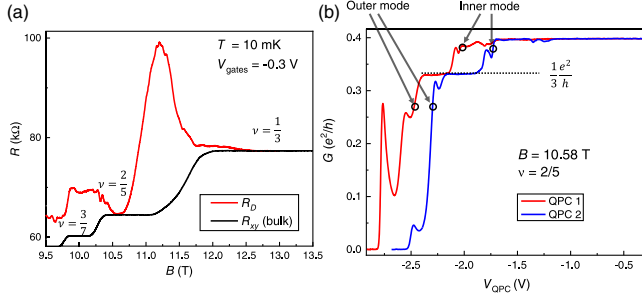


FIG. 2. (a) Diagonal resistance R_D measured across the interferometer with the 2DEG under the gates just depleted so that current flows through the device (red), compared to bulk transport R_{xy} (black). While R_D is generally larger than R_{xy} due to scattering induced within the device, at $\nu = 1/3$ and $\nu = 2/5$ there are regions where R_D reaches the bulk value of R_{xy} , indicating full transmission of the edge states with minimal scattering through the middle of the interferometer. (b) Conductance measured across the interferometer as a function of the QPC voltage for each individual QPC at $\nu = 2/5$, $B = 10.58$ T. The conductance starts at the full value of $G = 2/5 (e^2/h)$, and decreases as more negative voltage is applied to bring the edges together and induce backscattering. A clear intermediate plateau at $G = 1/3 (e^2/h)$ is visible, indicating full reflection of the inner edge while the outer edge state is fully transmitted. Approximate operating points for interference of the inner and outer modes are indicated with circles and arrows.

IV. INTERFERENCE OF THE OUTER MODE

We begin our analysis with examination of interference at $\nu = 2/5$ by considering the outer edge mode. Figure 3 shows conductance oscillations with the QPCs tuned to weakly backscatter the outer edge mode [with approximately 85% transmission for the outer edge mode; approximate operating points are indicated in Fig. 2(b)]. There is a central region where lines of constant phase follow a negative slope, indicative of Aharonov-Bohm interference, with lines of constant phase becoming nearly flat at higher and lower field. This behavior is very similar to interference observed at $\nu = 1/3$, where the transitions from AB interference to nearly flat lines of constant phase are caused by transitions from an incompressible to a compressible bulk; in the compressible regions, quasiparticles and quasiholes are removed and created with Φ_0 period. The fact that the outer edge mode interference at $\nu = 2/5$ exhibits a similar phenomenon indicates that this edge mode has the same properties as the single-edge state at $\nu = 1/3$, in agreement with theoretical expectations [35,55] and recent experiments probing the outer edge at $\nu = 2/5$ [21–23,63]. In the composite fermion model [5–7], this similarity can be understood from the fact that both the $\nu = 1/3$ edge state and the outer edge state at $\nu = 2/5$ are generated from the lowest Lambda level, and therefore are expected to have the same properties. While the localized quasiparticles of the bulk $2/5$ state have charge $e/5$, as discussed in

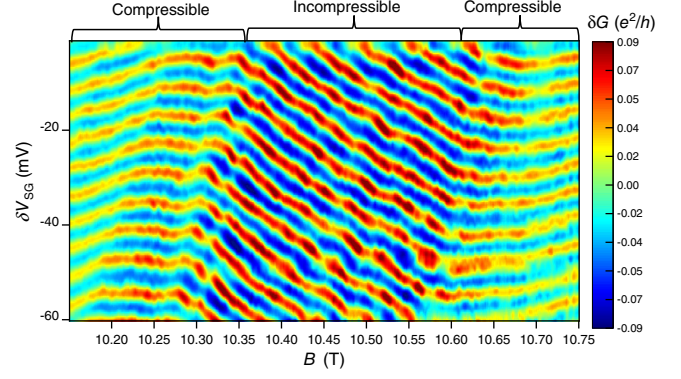


FIG. 3. Conductance oscillations versus B and δV_{SG} for the outer mode at $\nu = 2/5$. The oscillations resemble those observed at $\nu = 1/3$, with a central incompressible region with negatively sloped lines of constant phase, and the lines of constant phase becoming nearly flat at higher and lower fields when the density of states in the center of the device is high. Discrete jumps in phase due to changing quasiparticle number are less clearly identifiable than at $\nu = 1/3$.

Ref. [55], when the inner mode is fully reflected (resulting in a filling factor $\nu \leq 1/3$ in the QPCs), it is expected that the overall charge inside the device should be quantized in units of $e/3$ [35,55], and thus, the relevant θ_a in Eq. (1) is $2\pi/3$ since the localized inner puddle with $\Delta\nu = 1/5$ can be considered to be composed of charge $e/3$ anyon quasiparticles.

While the outer edge state at $\nu = 2/5$ shares properties with the $\nu = 1/3$ edge state, the properties of the bulk are different, which leads to some differences in the interference behavior. The energy gap of the $\nu = 2/5$ state is significantly smaller than $\nu = 1/3$, leading to a narrower region of magnetic field where the device exhibits negatively sloped incompressible-regime oscillations [64]. We measure an activated transport energy gap $\Delta^{2/5} = 3.6$ K at $\nu = 2/5$; based on the model of Rosenow and Stern [64], the range of field where the bulk is incompressible should be given by $\Delta B_{inc} = (\Delta\Phi_0 C / \nu e^* e^2)$, with $C \approx 4.4 \times 10^{-3} \frac{F}{m^2}$ the combined capacitance per unit area of the screening layers and $\Delta = 3.6$ K the energy gap. Using measured parameters for our device, this yields an expected incompressible region of approximately 430 mT, in reasonable agreement with our observed region of approximately 300 mT where the outer mode exhibits negatively sloped oscillations.

There are additional important differences in behavior between the single-edge mode at $\nu = 1/3$ and the outer mode at $\nu = 2/5$. At $\nu = 2/5$, even when the inner puddle is gapped and incompressible, the edge of the inner puddle remains gapless. Thus, charge can be added to the inner edge mode when the magnetic field and gate voltage are varied, resulting in changes in the inner puddle. Because of disorder, even in the interior of the incompressible inner

puddle there will be a finite density of localized $e/5$ quasiparticle states such that when B and δV_{SG} are varied, these localized states are occupied. The addition of an $e/5$ quasiparticle combined with a small change in charge on the edge of the inner puddle can result in a change in the overall number of $e/3$ quasiparticles by one, resulting in a phase jump for the outer edge. However, whether this change in quasiparticle number occurs at a particular value of gate voltage and magnetic field will depend sensitively on the energy function and interaction parameters within the device. While at $\nu = 1/3$, transitions in the number of localized quasiparticles were seen to occur along nearly straight positively sloped lines in the B - δV_{SG} plane [18,19] (since each $e/3$ quasiparticle is localized at a particular point in the bulk), at $\nu = 2/5$ the charge of the $e/3$ quasiparticles is divided among the localized $e/5$ quasiparticles, the condensate charge, and charge at the edge of the inner puddle, and so the dependence of N_{QP} on B and δV_{SG} will be more complicated. Figure 3 does show modulations in the incompressible region, which likely correspond to the creation of localized quasiparticles and modulations of θ via θ_a , although it might be considered that the $e/3$ quasiparticles have “lost their identity” [55] in forming the inner condensate.

To further investigate the correspondence between the outer mode at $\nu = 2/5$ and the edge mode at $\nu = 1/3$, we monitor interference over the entire range of magnetic field from $\nu = 2/5$ to $\nu = 1/3$ as shown in Fig. 4(d). The progression in the state of the interferometer from $\nu = 2/5$ to $\nu = 1/3$ is sketched in Figs. 4(a)–4(c). Because the QPC voltage required to weakly backscatter the outer mode at $2/5$ is slightly more negative than the voltage required to backscatter the single-edge state at $\nu = 1/3$ (likely due to the outer edge state moving inward as field is increased and the inner edge state vanishes), for this measurement we continuously adjust the QPC voltages as B is varied in order to maintain interference. QPC 1 is varied from -2.35 V at $\nu = 2/5$ to -2.17 V at $\nu = 1/3$, and QPC 2 is varied from -2.25 V at $\nu = 2/5$ to -2.07 V at $\nu = 1/3$. Bulk magneto-transport is shown in Fig. 4(e). The oscillations are continuous from $\nu = 2/5$ to $\nu = 1/3$, verifying that the edge state persists in both quantum Hall states.

Interestingly, while at both $\nu = 1/3$ and $\nu = 2/5$ the lines of constant phase become nearly flat above and below the incompressible region, in the transition region between $\nu = 2/5$ and $\nu = 1/3$ the lines adopt a shallow positive slope and interference is greatly suppressed. While positive slope is frequently associated with strong bulk-edge coupling effects in interferometers, when the outermost edge is being interfered, Coulomb effects generally result in zero slope rather than positive slope [36,47,55], so bulk-edge coupling cannot easily explain the positive slope in this transition region. A possible explanation for the positive slope is that in this range of magnetic field the area enclosed by the edge state shrinks, since it transitions from being an

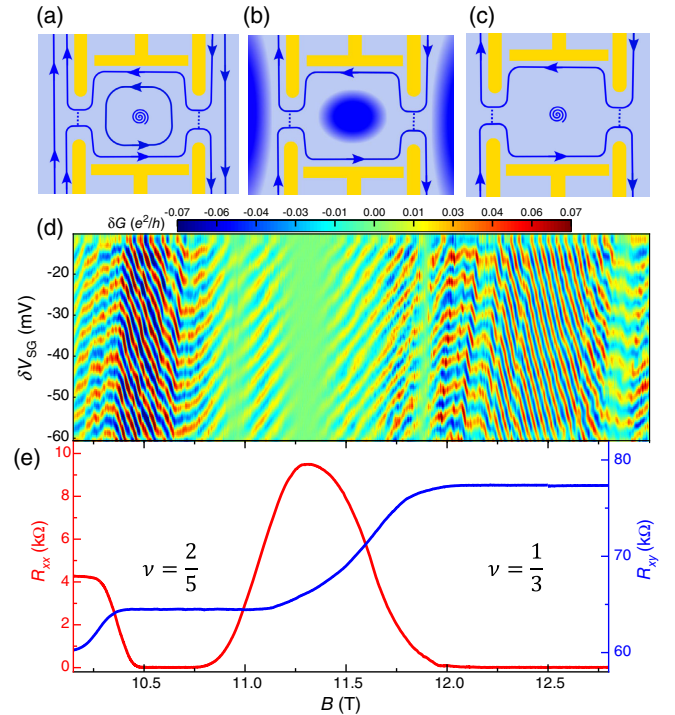


FIG. 4. (a) Schematic of outer mode interference at $\nu = 2/5$. (b) Schematic of interference in the highly compressible region midway between $\nu = 2/5$ and $\nu = 1/3$. (c) Schematic of interference of the single edge at $\nu = 1/3$. (d) Interference of the outer edge mode spanning filling factor $\nu = 2/5$ to $\nu = 1/3$ [panel (d)] compared to bulk transport R_{xx} and R_{xy} [panel (e)]. The conductance oscillations are largely continuous from $\nu = 2/5$ to $\nu = 1/3$. The QPCs are continuously adjusted as magnetic field is varied in order to maintain weak backscattering. There is a clear suppression of interference amplitude in the region where R_{xx} has a peak between $\nu = 2/5$ and $\nu = 1/3$, suggesting that high conductivity in the bulk suppresses interference. Interference at $\nu = 1/3$ is consistent with previous works [17–19], with a wide incompressible region with a small number of discrete phase jumps due to anyonic statistics, with the lines of constant phase flattening out at high and low field when the bulk becomes compressible.

outer edge state to being the only edge state in the system, which might cause it to move slightly inward. In other words, the position of the incompressible strip of filling $\nu = 1/3$, which forms the interior boundary of the $1/3$ edge mode, moves inward until it merges into a global filling of $\nu = 1/3$ in the central puddle [65]. The magnetic field period in the positively sloped region is approximately 92 mT, corresponding to approximately $8\Phi_0$; this is a relatively weak magnetic field dependence. The gate period is approximately 6 mV, nearly the same as in the incompressible regions on the flanks of $\nu = 2/5$ and $\nu = 1/3$. It is also noteworthy that in this transition region the interference amplitude is dramatically suppressed. This may occur because in this region, the bulk of the 2DEG is highly conductive (as can be seen from the large peak in R_{xx}), leading to significant smearing of the localized

quasiparticle number as the transitions are broadened [40], as well as a less well-defined interference path.

At $\nu = 1/3$, we observe behavior consistent with our previous experiments: There is a wide incompressible region where the device exhibits negatively sloped AB interference with a few discrete jumps in phase, with lines of constant phase flattening out at lower and higher magnetic fields when the bulk becomes compressible. More data at $\nu = 1/3$ are shown in Supplemental Material Fig. 8 and discussed in Sec. VIII [59]. The width of the incompressible region is approximately 600 mT, approximately a factor of 2 larger than at $\nu = 2/5$, reflecting the larger energy gap of the state.

V. INTERFERENCE OF THE INNER MODE

In Fig. 5(c), we show conductance as a function of the side-gate-voltage variation δV_{SG} (this side-gate-voltage variation is relative to -1.8 V and applied symmetrically to both side gates) and magnetic field B with the QPCs tuned to weak backscattering of the inner mode [both QPCs initially tuned to approximately 75% transmission of the inner mode; approximate operation points shown in Fig. 2(b)]. A schematic of this interference process is shown in Fig. 5(a).

In contrast to the relatively simple behavior of $\nu = 1$ where clear lines of constant phase follow a negative slope, for $\nu = 2/5$ the behavior is not a simple sinusoidal function of B and δV_{SG} . Instead, there are many discrete jumps in phase [indicated with dashed lines in Fig. 6(a)], which follow a positive slope in the B and δV_{SG} plane. These discrete jumps in phase create a checkerboardlike pattern in the conductance. It is also noteworthy that the amplitude is small, approximately an order of magnitude smaller than interference of the outer mode at $\nu = 2/5$ or at $\nu = 1/3$; this hints that interference of the edge mode is significantly more prone to decoherence [40]. Nevertheless, the interference pattern is temporally stable and repeatable in subsequent scans (see Supplemental Material Fig. 3 and Sec. III [59]).

The positive slope of the transition lines of the discrete jumps [dashed line in Fig. 6(a)] in the B - V_{SG} plane is consistent with previous observations of anyonic statistics for the $\nu = 1/3$ state. If the side gates coupled only to the edge states, then the gates would not affect the localized quasiparticle number, and the discrete jumps would be vertical (occurring only as a function of B). However, real devices have some coupling of the side gate to the bulk, leading to an excess bulk charge $\delta q_b = (\nu \bar{A} \delta B / \Phi_0) - \alpha_{\text{bulk}} \delta V_{SG} + e^* N_{QP}$, causing the contours of fixed bulk charge (across which, quasiparticle transitions happen) to have slope $(dV_{SG}/dB) = (\nu \bar{A} / \Phi_0 \alpha_{\text{bulk}}) \approx 0.64$ mV/mT. The observed slope is approximately 0.8 mV/mT, close to the value calculated from these simple charge balance considerations.

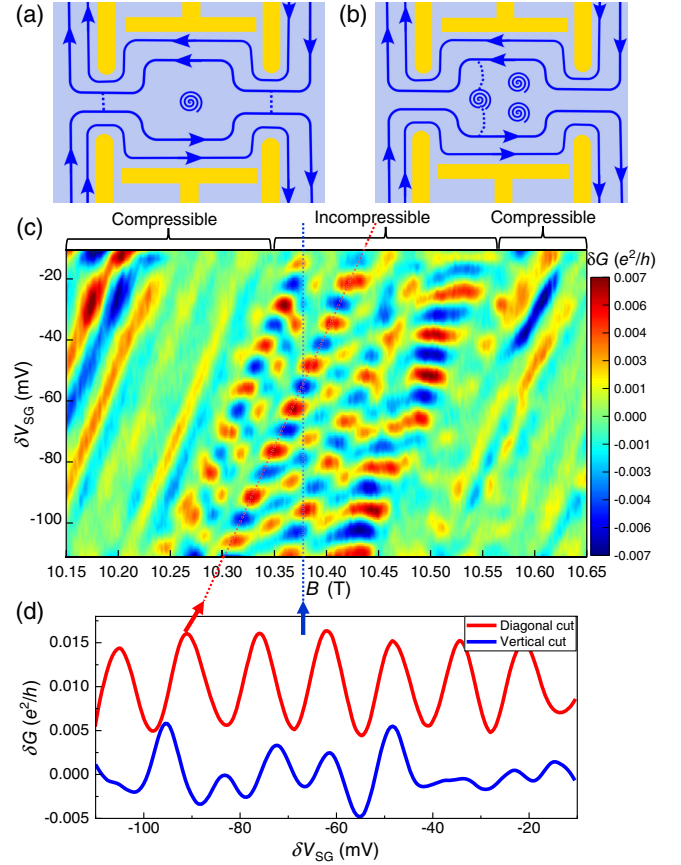


FIG. 5. (a) Schematic of interference for the inner mode at $\nu = 2/5$. (b) Schematic of resonant tunneling when the bulk is compressible and many quasiparticles are present inside the interferometer. (c) Conductance versus B and δV_{SG} for the inner mode at $\nu = \frac{2}{5}$. There is a central region where a checkerboard pattern forms with discrete jumps in the oscillation pattern indicative of anyonic statistics. At higher and lower magnetic fields where the bulk becomes compressible, the interference oscillations disappear, and weak positively sloped oscillations occur, which are most likely explained by conduction through the bulk rather than an interference process. (d) Vertical cut of conductance versus δV_{SG} (blue) in the incompressible regime. Since this cut intersects several of the discrete jumps in phase, the behavior is nonsinusoidal. On diagonal cuts parallel to (but in between) the discrete jumps in phase (red), the quasiparticle number is fixed, so the conductance oscillates sinusoidally due to the continuously varying Aharonov-Bohm phase. Red and blue dashed lines in (a) indicate where each cut is taken.

Vertical cuts of conductance versus δV_{SG} at fixed B [indicated with the blue arrow in Fig. 5(c), plotted in blue in Fig. 5(d)] show nonsinusoidal behavior due to the discrete jumps in phase. In stark contrast, line cuts parallel to (but in between) the discrete jumps in phase [indicated by the red arrow in Fig. 5(c), plotted in red in Fig. 5(d)] do show clear sinusoidal oscillations, indicating that along these contours the number of localized quasiparticles is fixed, and the phase variation is only due to the continuously varying Aharonov-Bohm phase in Eq. (1).

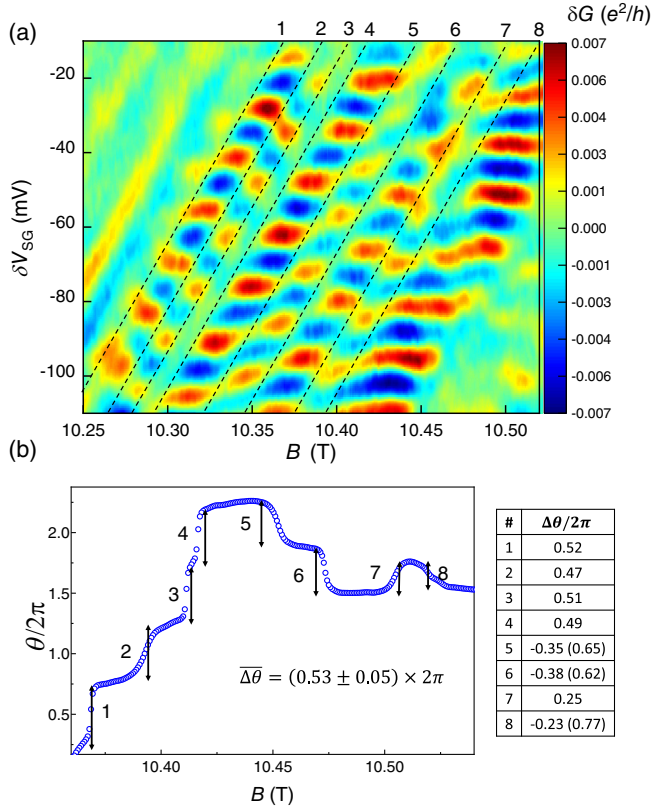


FIG. 6. (a) Conductance versus side gate voltage and magnetic field for the inner mode at $\nu = \frac{2}{5}$ [enlarged view of the incompressible region from Fig. 5(c)] with dashed lines indicating the positions of discrete jumps in phase. (b) Phase extracted via Fourier transform versus magnetic field. Discrete steps in the phase correspond to the discrete jumps visible in (a). The values of each phase jump (calculated from the difference of θ on each plateau between the jumps) are indicated in the table to the right of the plot.

VI. FRACTIONAL CHARGE

In regions between the discrete jumps, where the phase varies only due to the Aharonov-Bohm contribution, the gate-voltage oscillation period is approximately 14 mV. With the gate lever arm $(\partial\bar{A}/\partial V_{\text{SG}}) = 0.11 \mu\text{m}^2 \text{V}^{-1}$, this implies a flux period of approximately $4\Phi_0$ if bulk-edge coupling is neglected. To quantitatively extract the effective quasiparticle charge, we must account for both the change in area due to direct coupling of the gate to the edge and the effect of bulk-edge coupling from Eq. (2). This analysis yields the following equation for the gate-voltage oscillation period ΔV_{SG} when the bulk is incompressible:

$$\Delta V_{\text{SG}} = \frac{\Phi_0}{Be^*} \left(\frac{\partial\bar{A}}{\partial V_{\text{SG}}} + \frac{\kappa\alpha_{\text{bulk}}\Phi_0}{\Delta\nu B} \right)^{-1}, \quad (3)$$

where $\alpha_{\text{bulk}} = (\partial\bar{q}_b/\partial V_{\text{SG}})$ and $\kappa = -(\delta q_i/\delta q_b)$. $\kappa = 0.17$ is extracted for our device from finite bias conductance measurements (see Supplemental Material Fig. 6

and Secs. 6 and 7 [59] and Refs. [66–75]) and $\alpha_{\text{bulk}} = 0.06 \text{ mV}^{-1}$ is determined with the aid of zero magnetic field Coulomb blockade spectroscopy (see Supplemental Material Sec. II [59]). Applied to our device with $\Delta V_{\text{SG}} = 14 \text{ mV}$, Eq. (3) yields $e^* = 0.17 \pm 0.02$ for the inner mode (here, uncertainty is estimated from the FWHM of the Fourier-transform peak), close to the theoretical value of $e/5$. This confirms the interference of fractionally charged quasiparticles at $\nu = 2/5$ and supports previous measurements of fractional charge at $\nu = 2/5$ [56].

It is noteworthy that in the regions between the discrete jumps where the quasiparticle number is constant, the phase evolves with gate voltage but appears to be nearly independent of magnetic field [as shown in Fig. 6(b)]. This contrasts with the naive expectations of Eq. (1), which would imply a phase evolution with B and Φ_0/e^* oscillation period. On the other hand, Eq. (2) implies that in the incompressible region where N_{QP} is fixed, there will be a crossover from negatively sloped AB oscillations to positively sloped oscillations at a critical value of $\kappa = (\Delta\nu/\nu_{\text{in}}) = \frac{(1/15)}{(2/5)} = \frac{1}{6}$; this κ corresponds to the transition from the Aharonov-Bohm to the Coulomb-dominated regime for $\nu = 2/5$, and also applies to the regime of a compressible bulk. Note that a significantly larger bulk-edge coupling parameter is required for integer quantum Hall states to transition from Aharonov-Bohm to Coulomb-dominated interference, with the critical value being $\kappa = 0.5$.

This critical value of $\frac{1}{6}$ for $\nu = 2/5$ is very close to the value of $\kappa = 0.17$ from finite-bias measurements; thus, bulk-edge coupling does account for the weak B dependence in the incompressible regions between the discrete jumps. It is interesting to note that while the intrinsic bulk-edge coupling quantified by κ is not particularly strong, its impact at $\nu = 2/5$ is significant. Simulations of interference for the inner mode illustrating this effect for different values of κ are shown in Supplemental Material Fig. 3 and discussed in Sec. III [59].

Next we discuss in detail the discrete jumps in phase, which are indicated with dashed lines in Fig. 6(a). Qualitatively, these discrete jumps in phase are more dramatic features than the anyonic phase jumps which have been previously observed at $\nu = 1/3$ [18,19], consistent with the larger magnitude of θ_a at $\nu = 2/5$ compared to $\nu = 1/3$. In Fig. 6(b), we plot the interference phase versus magnetic field (the phase is extracted via Fourier-transform along diagonal cuts of conductance; see Supplemental Material Fig. 4 and Sec. IV [59]). Steps in the phase occur corresponding to the discrete jumps indicated in Fig. 6(a). Since there is weak magnetic field dependence in the regions between the jumps, the Aharonov-Bohm contribution to the phase is small, so the steps in phase correspond primarily to the transitions in quasiparticle

number (this is supported by the fact that the phase is nearly flat in the regions between the discrete jumps, even without subtracting an AB component). The values of the phase jumps (calculated as the difference in average phase on the plateaus on either side of the jump) are listed in the table inset in Fig. 6(b). Interestingly, there are both positive and negative jumps in phase, in contrast to the naive expectation of $\Delta\theta = -\theta_a = (4\pi/5)$ in the absence of bulk-edge coupling (the negative sign comes from the fact that increasing B is expected to remove quasiparticles or equivalently add quasiholes). The presence of both positive and negative jumps in phase indicates that bulk-edge coupling, even at $\kappa \simeq 0.17$, is indeed an important factor.

VII. QUASIPARTICLE STATISTICS

With bulk-edge coupling, the change in interference phase when a quasiparticle is removed based on Eq. (2) is $\Delta\theta = -\theta_a + \kappa[(e^*)^2/\Delta\nu]$; for the inner mode of $\nu = 2/5$ with $e^* = 1/5$, $\Delta\nu = 2/5 - 1/3 = 1/15$, and $\theta_a = (-4\pi/5)$, this yields

$$\frac{\Delta\theta}{2\pi} = -\frac{\theta_a}{2\pi} + \kappa \frac{(e^*)^2}{\Delta\nu} = \left(\frac{2}{5} + \kappa \frac{3}{5}\right). \quad (4)$$

The factor of $1/\Delta\nu$ makes interference at $\nu = 2/5$ significantly more sensitive to bulk-edge coupling than at $\nu = 1/3$. This implies that a moderate bulk-edge coupling parameter of $\kappa = \frac{1}{6}$ (the same critical value as for the Aharonov-Bohm slope) can push $\Delta\theta$ to the transition point of $0.5 \times 2\pi$, where the phase jumps cross over from positive to negative. Thus, our observation of a mix of positive and negative phase jumps may be explained by an average bulk-edge coupling parameter of $\kappa \approx \frac{1}{6} \approx 0.167$, with small variations in the exact coupling of individual localized quasiparticle states to the edge leading to some quasiparticle transitions giving a positive change in phase and some negative (with the phase defined from $-\pi$ to $+\pi$). On the other hand, based on Eq. (4), it is more convenient to define jumps in phase from 0 to 2π in order to quantitatively account for the effect of bulk-edge coupling. The values of the discrete jumps are listed in the inset of Fig. 6(b); for the negative jumps, the value shifted into the range 0 to 2π is shown in parentheses. We calculate the average $\Delta\bar{\theta}$ using the values from 0 to 2π , which yields $\Delta\bar{\theta} = (0.53 \pm 0.05) \times 2\pi$ (note that the standard deviation is $0.15 \times 2\pi$, and the uncertainty is estimated by the standard error). This average value is somewhat higher than the ideal value of $\Delta\theta = -\theta_a = (4\pi/5)$, but as indicated by Eq. (4), finite bulk-edge coupling tends to increase $\Delta\theta$, so an experimental value somewhat higher than the ideal value is expected.

Based on Eq. (4), the anyonic phase can be extracted from the phase jumps as $\theta_a = -\Delta\bar{\theta} + 2\pi\kappa[(e^*)^2/\Delta\nu]$.

Using the value of $\kappa = 0.17$ extracted from finite bias measurements yields $\theta_a = -(0.43 \pm 0.05) \times 2\pi$, in good agreement with the value of $\theta_a = -(4\pi/5)$ predicted from theory [4,35,55,57] and numerical work [58,61]. Thus, our experiment confirms the theoretical prediction of anyonic braiding statistics at $\nu = 2/5$ with statistical angle $\theta_a = -(4\pi/5)$. This is the first quantitative experimental determination of the anyonic braiding phase at the hierarchy $\nu = 2/5$ state.

VIII. BEHAVIOR IN THE COMPRESSIBLE REGIME

As can be seen in Fig. 5(c), there is a limited range of field where the checkerboard pattern of interference created by discrete jumps in phase is visible; above and below this region there are weak oscillations with a large magnetic field period (corresponding to approximately $4\Phi_0$) and a positive slope in the B - ΔV_{SG} plane. The values of magnetic field where these transitions occur are similar to those where the bulk transitions from incompressible to compressible when interfering the outer mode, as seen in Fig. 3, suggesting that the transition in behavior also occurs due to the bulk becoming compressible. Coulomb-dominated interference [36,44,46,55] can result in positively sloped oscillations in both compressible and incompressible regimes. However, the positive-slope oscillations in the compressible regions are not consistent with interference in the fully compressible regime. With a fully compressible bulk, an $e/5$ quasiparticle or quasihole would be added or removed with each $\Phi_0/2$ increase in flux in order to keep the density of the 2DEG constant. This would result in oscillations with Φ_0 magnetic field period based on Eq. (1) (the lines of constant phase could be positive or negative depending on the degree of bulk-edge coupling, but this Φ_0 period would remain the same), much smaller than observed.

Additionally, the expected slope of Coulomb-dominated oscillations would be smaller than what is observed, with the steepest possible slope being for $\kappa = 1$, for which Eq. (3) yields $\Delta V_{SG} \approx 4.4$ mV and $\Delta B = \Phi_0 \approx 11.5$ mT, yielding a slope of 0.38 mV/mT (this would also be the slope for Coulomb-dominated compressible-regime interference). This slope is far smaller than the slope of 0.8 mV/mT of the observed oscillations in the compressible region, giving additional support for the fact that these oscillations cannot be explained by Coulomb-dominated interference.

The observed slope approximately equal to 0.8 mV/mT is close to the value of the slope of the quasiparticle transitions seen in Fig. 6(a). This suggests that the peaks in conductance correspond a Coulomb-blockaded resonant tunneling process through the middle of the interferometer (similar to process ii in Ref. [36]) rather than a true interference process where tunneling occurs only at the QPCs; this possible process is illustrated in Fig. 5(b). In this process, conductance peaks occur when a particular

quasiparticle state in the bulk becomes resonant with chemical potential, and since the change in energy of these states depends most acutely on the electrostatic charging energy, contours of constant conductance would be expected to follow the same slope as lines of constant excess bulk charge, i.e., $(dV_{SG}/dB) = (\nu\bar{A}/\Phi_0\alpha_{\text{bulk}}) \approx 0.64$ mV/mT, which is the same slope as for the quasiparticle transition lines. The oscillation periods would depend on what fraction of quasiparticle states couple strongly enough to both the upper and lower edges of the interferometer to exhibit a conductance resonance; the relatively large and somewhat irregular period may suggest that this applies to only a fraction of quasiparticle states in the bulk.

This bulk contribution to conductance is consistent with the observation from Fig. 2(a) that conductance through the device is quantized only in a very narrow window of magnetic field even when minimal backscattering is induced in the QPCs. On the other hand, the absence of compressible-regime interference for the inner mode is interesting, given that the outer mode does show interference in this regime. A possible explanation for this is thermal smearing of the quasiparticle number, leading to topological dephasing [76]. A rapid suppression of amplitude with the temperature was previously observed at $\nu = 1/3$ in the compressible regime due to this mechanism [18] (note also that for the outer mode at $\nu = 2/5$, the amplitude is significantly suppressed in the compressible regimes as can be seen in Fig. 3). For the inner mode at $\nu = 2/5$, the relevant energy scale for confining quasiparticles should be much smaller due to the small quasiparticle charge $e/5$, making it plausible that the oscillations are so strongly thermally smeared that they are not measurable. Even in the incompressible regime, we find a small temperature decay scale $T_0 = 26$ mK (see Supplemental Material Fig. 7 and Sec. VIII [59]), so it appears reasonable that interference is unmeasurable in the compressible regime where the temperature decay scale will be even smaller. This is supported by simulations (Supplemental Material Fig. 5 [59]).

IX. CONCLUSIONS

We measure conductance oscillations due to interference of the inner and outer edge modes at $\nu = 2/5$. The outer mode exhibits behavior similar to $\nu = 1/3$, supporting the expectation that the outer edge state at $\nu = 2/5$ has the same properties as the single-edge state at $\nu = 1/3$, although the smaller energy gap results in a narrower range of magnetic field over which the bulk is incompressible. The inner edge exhibits oscillations with a gate-voltage period consistent with an interfering charge $e^* = 0.17 \pm 0.02$, close to the theoretically predicted value of $\frac{1}{5}$. Discrete jumps in phase with average value $\bar{\Delta}\theta = 0.53$ are observed; after taking into account the impact of bulk-edge coupling, we extract an anyonic braiding phase

$\theta_a = (-0.43 \pm 0.05) \times 2\pi$, close to the theoretically anticipated value $\theta_a = -(4\pi/5)$. These measurements give experimental support to the theoretical prediction of anyonic quasiparticles at the $\nu = 2/5$ state, and demonstrate that Fabry-Pérot interferometry can be extended to fractional quantum Hall states with multiple edge modes to make quantitative measurements.

Note added in proof.—We note that θ_a as defined in Eq. (1) and measured in our interference experiment is twice the statistical angle θ that defines the phase acquired in a single exchange of anyon positions. Measurement of θ_a determines θ modulo π , not modulo 2π . We thank Nick Read for illuminating conversations on this point.

ACKNOWLEDGMENTS

This work was supported by the U.S. Department of Energy, Office of Science, Office of Basic Energy Sciences, under Award No. DE-SC0020138. We wish to thank Bert Halperin and Dima Feldman for several insightful discussions and suggestions that improved our manuscript.

-
- [1] D. C. Tsui, H. L. Stormer, and A. C. Gossard, *Two-Dimensional Magnetotransport in the Extreme Quantum Limit*, *Phys. Rev. Lett.* **48**, 1559 (1982).
 - [2] R. B. Laughlin, *Anomalous Quantum Hall Effect: An Incompressible Quantum Fluid with Fractionally Charged Excitations*, *Phys. Rev. Lett.* **50**, 1395 (1983).
 - [3] F. D. M. Haldane, *Fractional Quantization of the Hall Effect: A Hierarchy of Incompressible Quantum Fluid States*, *Phys. Rev. Lett.* **51**, 605 (1983).
 - [4] B. I. Halperin, *Statistics of Quasiparticles and the Hierarchy of Fractional Quantized Hall States*, *Phys. Rev. Lett.* **52**, 1583 (1984).
 - [5] J. K. Jain, *Composite-Fermion Approach for the Fractional Quantum Hall Effect*, *Phys. Rev. Lett.* **63**, 199 (1989).
 - [6] J. K. Jain, *Theory of the Fractional Quantum Hall Effect*, *Phys. Rev. B* **41**, 7653 (1990).
 - [7] J. K. Jain, *Composite Fermions* (Cambridge University Press, Cambridge, England, 2007).
 - [8] J. M. Leinaas and J. Myrheim, *On the Theory of Identical Particles*, *Nuovo Cimento Soc. Ital. Fis.* **37B**, 1 (1977).
 - [9] G. A. Goldin, R. Menikoff, and D. H. Sharp, *Particle Statistics from Induced Representations of a Local Current Group*, *J. Math. Phys.* **21**, 650 (1980).
 - [10] F. Wilczek, *Quantum Mechanics of Fractional-Spin Particles*, *Phys. Rev. Lett.* **49**, 957 (1982).
 - [11] D. Arovas, J. R. Schrieffer, and Frank Wilczek, *Fractional Statistics and the Quantum Hall Effect*, *Phys. Rev. Lett.* **53**, 722 (1984).
 - [12] V. J. Goldman and B. Su, *Resonant Tunneling in the Quantum Hall Regime: Measurement of Fractional Charge*, *Science* **267**, 1010 (1995).
 - [13] M. P. Rössli, M. Hug, G. Nicolí, P. Märki, C. Reichl, B. Rosenow, W. Wegscheider, K. Ensslin, and T. Ihn, *Frac-*

- tional Coulomb Blockade for Quasiparticle Tunneling between Edge Channels*, *Sci. Adv.* **7**, eabf5547 (2021).
- [14] L. Saminadayar, D. C. Glattli, Y. Jin, and B. Etienne, *Observation of the $e/3$ Fractionally Charged Laughlin Quasiparticle*, *Phys. Rev. Lett.* **79**, 2526 (1997).
- [15] R. De-Picciotto, M. Reznikov, M. Heiblum, V. Umansky, G. Bunin, and D. Mahalu, *Direct Observation of a Fractional Charge*, *Nature (London)* **389**, 162 (1997).
- [16] J. Martin, S. Ilani, B. Vardene, J. Smet, V. Umansky, D. Mahalu, D. Schuh, G. Abstreiter, and A. Yacoby, *Localization of Fractionally Charged Quasi-Particles*, *Science* **305**, 980 (2004).
- [17] J. Nakamura, S. Fallahi, H. Sahasrabudhe, R. Rahman, S. Liang, G. C. Gardner, and M. J. Manfra, *Aharonov-Bohm Interference of Fractional Quantum Hall Edge Modes*, *Nat. Phys.* **15**, 563 (2019).
- [18] J. Nakamura, S. Liang, G. C. Gardner, and M. J. Manfra, *Direct Observation of Anyonic Braiding Statistics*, *Nat. Phys.* **16**, 931 (2020).
- [19] J. Nakamura, S. Liang, G. C. Gardner, and M. J. Manfra, *Impact of Bulk-Edge Coupling on Observation of Anyonic Braiding Statistics in Quantum Hall Interferometers*, *Nat. Commun.* **13**, 344 (2022).
- [20] H. Bartolomei, M. Kumar, R. Bisognin, A. Marguerite, E. Bocquillon, A. Cavanna, Q. Dong, U. Gennser, and Y. Jin, *Fractional Statistics in Anyon Collisions*, *Science* **368**, 173 (2020).
- [21] M. Ruelle, E. Frigerio, J. M. Berroir, B. Plaçaïs, J. Rech, A. Cavanna, U. Gennser, Y. Jin, and G. Fève, *Comparing Fractional Quantum Hall Laughlin and Jain Topological Orders with the Anyon Collider*, *Phys. Rev. X* **13**, 011031 (2023).
- [22] P. Glidic, O. Maillet, A. Aassime, C. Piquard, A. Cavanna, U. Gennser, Y. Jin, A. Anthore, and F. Pierre, *Cross-Correlation Investigation of Anyon Statistics in the $\nu = 1/3$ and $2/5$ Fractional Quantum Hall States*, *Phys. Rev. X* **13**, 011030 (2023).
- [23] H. K. Kundu, S. Biswas, N. Ofek, V. Umansky, and M. Heiblum, *Anyonic Interference and Braiding Phase in a Mach-Zehnder Interferometer*, *Nat. Phys.* **19**, 515 (2023).
- [24] I. Taktak, M. Kapfer, J. Nath, P. Roulleau, M. Acciai, J. Splettstoesser, I. Farrer, D. A. Ritchie, and D. C. Glattli, *Two-Particle Time-Domain Interferometry in the Fractional Quantum Hall Effect Regime*, *Nat. Commun.* **13**, 5863 (2022).
- [25] K. T. Law, D. E. Feldman, and Y. Gefen, *Electronic Mach-Zehnder Interferometer as a Tool to Probe Fractional Statistics*, *Phys. Rev. B* **74**, 045319 (2006).
- [26] V. V. Ponomarenko and D. V. Averin, *Mach-Zehnder Interferometer in the Fractional Quantum Hall Regime*, *Phys. Rev. Lett.* **99**, 066803 (2007).
- [27] D. E. Feldman and B. I. Halperin, *Fractional Charge and Fractional Statistics in the Quantum Hall Effects*, *Rep. Prog. Phys.* **84**, 076501 (2021).
- [28] D. E. Feldman and A. Kitaev, *Detecting Non-Abelian Statistics with an Electronic Mach-Zehnder Interferometer*, *Phys. Rev. Lett.* **97**, 186803 (2006).
- [29] S. A. Kivelson and V. L. Pokrovsky, *Methods to Measure the Charge of the Quasiparticles in the Fractional Quantum Hall Effect*, *Phys. Rev. B* **40**, 1373 (1989).
- [30] S. Kivelson, *Semiclassical Theory of Localized Many-Anyon States*, *Phys. Rev. Lett.* **65**, 3369 (1990).
- [31] C. de C. Chamon, D. E. Freed, S. A. Kivelson, S. L. Sondhi, and X. G. Wen, *Two Point-Contact Interferometer for Quantum Hall Systems*, *Phys. Rev. B* **55**, 2331 (1997).
- [32] E.-A. Kim, *Aharonov-Bohm Interference and Fractional Statistics in a Quantum Hall Interferometer*, *Phys. Rev. Lett.* **97**, 216404 (2006).
- [33] P. Bonderson, A. Kitaev, and K. Shtengel, *Detecting Non-Abelian Statistics in the $\nu = 5/2$ Fractional Quantum Hall State*, *Phys. Rev. Lett.* **96**, 016803 (2006).
- [34] A. Stern and B. I. Halperin, *Proposed Experiments to Probe the Non-Abelian $\nu = 5/2$ Quantum Hall State*, *Phys. Rev. Lett.* **96**, 016802 (2006).
- [35] A. Stern, *Anyons and the Quantum Hall Effect—A Pedagogical Review*, *Ann. Phys. (Amsterdam)* **323**, 204 (2008).
- [36] B. Rosenow and B. I. Halperin, *Influence of Interactions on Flux and Back-Gate Period of Quantum Hall Interferometers*, *Phys. Rev. Lett.* **98**, 106801 (2007).
- [37] A. Stern, B. Rosenow, R. Ilan, and B. I. Halperin, *Interference, Coulomb Blockade, and the Identification of Non-Abelian Quantum Hall States*, *Phys. Rev. B* **82**, 085321 (2010).
- [38] C. W. von Keyserlingk, S. H. Simon, and B. Rosenow, *Enhanced Bulk-Edge Coulomb Coupling in Fractional Fabry-Perot Interferometers*, *Phys. Rev. Lett.* **115**, 126807 (2015).
- [39] M. Carrega, L. Chirulli, S. Heun, and L. Sorba, *Anyons in Quantum Hall Interferometry*, *Nat. Rev. Phys.* **3**, 698 (2021).
- [40] D. E. Feldman and B. I. Halperin, *Robustness of Quantum Hall Interferometry*, *Phys. Rev. B* **105**, 165310 (2022).
- [41] Y. Ji, Y. Chung, D. Sprinzak, M. Heiblum, and D. Mahalu, *An Electronic Mach-Zehnder Interferometer*, *Nature (London)* **422**, 415 (2003).
- [42] E. V. Deviatov and A. Lorke, *Experimental Realization of a Fabry-Perot-Type Interferometer by Copropagating Edge States in the Quantum Hall Regime*, *Phys. Rev. B* **77**, 161302(R) (2008).
- [43] P. Roulleau, F. Portier, P. Roche, A. Cavanna, G. Faini, U. Gennser, and D. Mailly, *Direct Measurement of the Coherence Length of Edge States in the Integer Quantum Hall Regime*, *Phys. Rev. Lett.* **100**, 126802 (2008).
- [44] Y. Zhang, D. T. McClure, E. M. Levenson-Falk, C. M. Marcus, L. N. Pfeiffer, and K. W. West, *Distinct Signatures for Coulomb Blockade and Aharonov-Bohm Interference in Electronic Fabry-Perot Interferometers*, *Phys. Rev. B* **79**, 241304(R) (2009).
- [45] D. T. McClure, Y. Zhang, B. Rosenow, E. M. Levenson-Falk, C. M. Marcus, L. N. Pfeiffer, and K. W. West, *Edge-State Velocity and Coherence in a Quantum Hall Fabry-Pérot Interferometer*, *Phys. Rev. Lett.* **103**, 206806 (2009).
- [46] N. Ofek, A. Bid, M. Heiblum, A. Stern, V. Umansky, and D. Mahalu, *Role of Interactions in an Electronic Fabry-Perot Interferometer Operating in the Quantum Hall Effect Regime*, *Proc. Natl. Acad. Sci. U.S.A.* **107**, 5276 (2010).
- [47] D. T. McClure, W. Chang, C. M. Marcus, L. N. Pfeiffer, and K. W. West, *Fabry-Perot Interferometry with Fractional Charges*, *Phys. Rev. Lett.* **108**, 256804 (2012).

- [48] A. Kou, C. M. Marcus, L. N. Pfeiffer, and K. W. West, *Coulomb Oscillations in Antidots in the Integer and Fractional Quantum Hall Regimes*, *Phys. Rev. Lett.* **108**, 256803 (2012).
- [49] R. L. Willett, L. N. Pfeiffer, and K. W. West, *Measurement of Filling Factor $5/2$ Quasiparticle Interference with Observation of Charge $e/4$ and $e/2$ Period Oscillations*, *Proc. Natl. Acad. Sci. U.S.A.* **106**, 8853 (2009).
- [50] R. L. Willett, C. Nayak, K. Shtengel, L. N. Pfeiffer, and K. W. West, *Magnetic-Field-Tuned Aharonov-Bohm Oscillations and Evidence for Non-Abelian Anyons at $\nu = 5/2$* , *Phys. Rev. Lett.* **111**, 186401 (2013).
- [51] R. L. Willett, K. Shtengel, C. Nayak, L. N. Pfeiffer, Y. J. Chung, M. L. Peabody, K. W. Baldwin, and K. W. West, *Interference Measurements of Non-Abelian $e/4$ and Abelian $e/2$ Quasiparticle Braiding*, *Phys. Rev. X* **13**, 011028 (2023).
- [52] Y. Ronen, T. Werkmeister, D. Najafabadi, A. T. Pierce, L. E. Anderson, Y. J. Shin, S. Y. Lee, Y. H. Lee, B. Johnson, K. Watanabe, T. Taniguchi, A. Yacoby, and P. Kim, *Aharonov-Bohm Effect in Graphene Fabry-Perot Quantum Hall Interferometers*, *Nat. Nanotechnol.* **16**, 563 (2021).
- [53] C. Déprez, L. Veyrat, H. Vignaud, G. Nayak, K. Watanabe, T. Taniguchi, F. Gay, H. Sellier, and B. Sacépé, *A Tunable Fabry-Pérot Quantum Hall Interferometer in Graphene*, *Nat. Nanotechnol.* **16**, 555 (2021).
- [54] L. Zhao, E. G. Arnault, T. F. Larson, Z. Iftikhar, A. Seredinski, T. Fleming, K. Watanabe, T. Taniguchi, F. Amet, and G. Finkelstein, *Graphene-Based Quantum Hall Interferometer with Self-Aligned Side Gates*, *Nano Lett.* **22**, 9645 (2022).
- [55] B. I. Halperin, A. Stern, I. Neder, and B. Rosenow, *Theory of the Fabry-Perot Quantum Hall Interferometer*, *Phys. Rev. B* **83**, 155440 (2011).
- [56] M. Reznikov, R. De Picciotto, T. G. Griffiths, M. Heiblum, and V. Umansky, *Observation of Quasiparticles with One-Fifth of an Electron's Charge*, *Nature (London)* **399**, 238 (1999).
- [57] W. P. Su, *Statistics of the Fractionally Charged Excitations in the Quantum Hall Effect*, *Phys. Rev. B* **34**, 1031 (1986).
- [58] G. S. Jeon, K. L. Graham, and J. K. Jain, *Fractional Statistics in the Fractional Quantum Hall Effect*, *Phys. Rev. Lett.* **91**, 036801 (2003).
- [59] See Supplemental Material at <http://link.aps.org/supplemental/10.1103/PhysRevX.13.041012> for additional data, a table of symbols, analysis of interaction parameters, simulations, and data from additional devices B and C.
- [60] B. Blok and X. G. Wen, *Effective Theories of the Fractional Quantum Hall Effect: Hierarchy Construction*, *Phys. Rev. B* **42**, 8145 (1990).
- [61] G. S. Jeon, K. L. Graham, and J. K. Jain, *Berry Phases for Composite Fermions: Effective Magnetic Field and Fractional Statistics*, *Phys. Rev. B* **70**, 125316 (2004).
- [62] S. Birner, T. Zibold, T. Andlauer, T. Kubis, M. Sabathil, A. Trellakis, and P. Vogl, *NEXTNANO: General Purpose 3-D Simulations*, *IEEE Trans. Electron Devices* **54**, 2137 (2007).
- [63] J. Y. M. Lee, C. Hong, T. Alkalay, N. Schiller, V. Umansky, M. Heiblum, Y. Oreg, and H. Sim, *Partitioning of Diluted Anyons Reveals their Braiding Statistics*, *Nature* **617**, 277 (2023).
- [64] B. Rosenow and A. Stern, *Flux Superperiods and Periodicity Transitions in Quantum Hall Interferometers*, *Phys. Rev. Lett.* **124**, 106805 (2020).
- [65] D. B. Chklovskii, B. I. Shklovskii, and L. I. Glazman, *Electrostatics of Edge Channels*, *Phys. Rev. B* **46**, 4026 (1992).
- [66] M. P. Rössli, L. Brem, B. Kratochwil, G. Nicolí, B. A. Braem, S. Hennel, P. Märki, M. Berl, C. Reichl, W. Wegscheider, K. Ensslin, T. Ihn, and B. Rosenow, *Observation of Quantum Hall Interferometer Phase Jumps Due to a Change in the Number of Bulk Quasiparticles*, *Phys. Rev. B* **101**, 125302 (2020).
- [67] I. Sivan, H. K. Choi, J. Park, A. Rosenblatt, Y. Gefen, D. Mahalu, and V. Umansky, *Observation of Interaction-Induced Modulations of a Quantum Hall Liquid's Area*, *Nat. Commun.* **7**, 1 (2016).
- [68] G. A. Frigeri, D. D. Scherer, and B. Rosenow, *Sub-Periods and Apparent Pairing in Integer Quantum Hall Interferometers*, *Europhys. Lett.* **126**, 67007 (2019).
- [69] C. W. J. Beenakker, *Theory of Coulomb-Blockade Oscillations in the Conductance of a Quantum Dot*, *Phys. Rev. B* **44**, 1646 (1991).
- [70] L. P. Kouwenhoven and P. L. McEuen, *Single Electron Transport through a Quantum Dot*, in *Nanotechnology*, edited by G. Timp (Springer Science, New York, 1999), Chap. 13, pp. 471–535.
- [71] X. G. Wen, *Edge Transport Properties of the Fractional Quantum Hall States and Weak-Impurity Scattering of a One-Dimensional Charge-Density Wave*, *Phys. Rev. B* **44**, 5708 (1991).
- [72] O. Smits, J. K. Slingerland, and S. H. Simon, *Tunnelling Current through Fractional Quantum Hall Interferometers*, *Phys. Rev. B* **89**, 045308 (2013).
- [73] T. Fujisawa, *Nonequilibrium Charge Dynamics of Tomonaga-Luttinger Liquids in Quantum Hall Edge Channels*, *Ann. Phys. (Berlin)* **534**, 1 (2022).
- [74] D. B. Chklovskii, K. A. Matveev, and B. I. Shklovskii, *Ballistic Conductance of Interacting Electrons in the Quantum Hall Regime*, *Phys. Rev. B* **47**, 12605 (1993).
- [75] H. Sahasrabudhe, B. Novakovic, J. Nakamura, S. Fallahi, M. Povolotskyi, G. Klimeck, R. Rahman, and M. J. Manfra, *Optimization of Edge State Velocity in the Integer Quantum Hall Regime*, *Phys. Rev. B* **97**, 085302 (2018).
- [76] J. Park, Y. Gefen, and H. S. Sim, *Topological Dephasing in the $\nu = 2/3$ Fractional Quantum Hall Regime*, *Phys. Rev. B* **92**, 245437 (2015).